Laser Focusing of Atoms: A Particle Optics Approach

J. J. McClelland and M. R. Scheinfein*
Electron and Optical Physics Division
National Institute of Standards and Technology
Gaithersburg, MD 20899

January 14, 1991

*present address: Center for Solid State Science, Arizona State Univ., Tempe, AZ

Abstract

The use of a TEM_{01}^{*} ("donut") mode laser beam has been proposed as a means of focusing an atomic beam to nanometer scale spot diameters. We have analyzed the classical trajectories of atoms through a donut mode laser beam using methods developed for particle optics. The differential equation describing the first order paraxial lens properties has exactly the same form as the "bell-shaped" magnetic Newtonian lens first analyzed by Glaser for the focusing of electrons in an electron microscope objective. We calculate the first order properties of the lens, obtaining cardinal elements valid over the entire operating range of the lens, including the "thick" and immersion regimes. Contributions to the ultimate spot size are discussed, including four aberrations plus diffraction and atom beam collimation effects. Explicit expressions for spherical, chromatic, spontaneous emission, and dipole fluctuation aberrations are obtained. Examples are discussed for a sodium atomic beam, showing that sub-nanometer diameter spots may be achieved with reasonable laser and atom beam parameters. Optimization of the lens is also discussed.

1 Introduction

The influence of near-resonant laser light on the motion of atoms in free space has generated a significant amount of interest over the past few years. In particular, it has been suggested, and in some ways demonstrated,[1, 2, 3] that an atom beam can be focused using the forces exerted on the atoms by the laser light. The ability to focus atom beams suggests a number of interesting applications, including atomic microscopy, microfabrication, and precise control of atomic beams for precision measurements. Two major considerations in the practical applicability of laser-atom focusing are the ease with which the focusing process can be modeled, and the ultimate resolution attainable. In this paper, we show that for coaxial focusing in a TEM_{01}^{*} laser beam, the first order (paraxial) focal properties can be exactly modeled analytically. We also discuss all the major aberrations to show that diffraction limited spots of order 1 nm can in principle be obtained.

An atom in the radiation field of a near-resonant laser experiences two types of force.[4] The spontaneous emission force results from the absorption and random spontaneous emission of photons. This random process is limited by the rate at which spontaneous emission occurs, and saturates as the laser intensity increases. The second type of force, the dipole force, is a result of the interaction of the induced atomic dipole with a gradient in laser beam intensity. This interaction can be made large by increasing the intensity gradient within the laser beam, and by increasing the detuning of the laser frequency from the natural resonance frequency of the atom. In the case of positive detuning, when the laser frequency is greater than the atomic resonance frequency, the force on the atoms is from the region of higher laser intensity towards lower laser intensity. The opposite is true for negative detuning, i.e., the force

is toward higher intensity.

In 1978, Bjorkholm et al.[1] demonstrated that an atom beam propagating coaxially with a Gaussian (TEM_{00}) laser beam could be focused to about 250 μm making use of the dipole force. Negative detuning was used so that the atoms were attracted to the higher laser intensity in the center of the beam. In a subsequent paper[2], they showed that a spot size of 28 μm could be obtained, and examined the limitations on the ultimate spot size imposed by spontaneous emission processes. In 1988, Balykin et al.[3] reported experiments using a lens made up of two counter-propagating, diverging, Gaussian laser beams oriented transversely to the atom beam. They were able to obtain the image of two atomic sources, demonstrating real image formation with a laser-atom lens. While these experiments represent important pioneering work, both methods of focusing atoms suffer from the same problem if one is concerned with ultimate resolution. In each case, the atoms travel through regions of high laser intensity, where a significant amount of spontaneous emission occurs. This acts to increase the amount of random motion in the atomic beam, which effectively decreases the resolution.

Balykin and Letokhov[5] first analyzed the properties of a laser-atom lens consisting of an atom beam travelling coaxially through the focus of a TEM_{01}^{*} laser beam (see Fig. 1). Positive detuning is used, so the force is toward the hollow center of the laser beam. This type of lens has the advantage that the atoms go through a relatively low intensity region, so spontaneous emission is kept to a minimum. Balykin and Letokhov treated the lens in the thin lens approximation, and analyzed the focal length, spherical aberration, chromatic aberration, and the effects of spontaneous emission on the spot size. Their approach was a wave-optical one, in which the atom

propagation was treated by considering the phase change of a de Broglie wavefront on passing through the lens. Diffraction of the atoms was thus included inherently in their approach. They found that for reasonable laser and atom beam parameters, spot sizes of a fraction of a nanometer could be obtained.

Recently, Gallatin and Gould[6] extended the wave optical approach of Balykin and Letokhov to correctly treat the lens as a thick lens. They used path integral formalism to solve Schrödinger's equation for the propagation of a Gaussian atom beam in the TEM_{01}^{*} laser field, obtaining focal spot sizes and positions of optimum focus for a number of realistic cases. They also estimated, in the thin lens limit, the effects of spherical aberration, chromatic aberration, spontaneous emission and dipole fluctuations. They found that, in contrast to the result of Balykin and Letokhov, spherical aberration does not vanish for a particular set of laser beam parameters. Further, they found the largest contributions to the spot size to be diffraction, spherical aberration and dipole fluctuations. Spot sizes of several nanometers were calculated for the cases they examined.

Our approach to the analysis of the donut mode laser-atomic lens is to treat the atoms as classical particles moving in the potential generated by the dipole force. We make use of methods, originally developed for charged particle optics, for calculating the trajectories of particles in cylindrically symmetric potential fields. Applied to the donut mode laser-atomic lens, these methods result in a very simple understanding of the first order focal properties. In fact, the first order paraxial equation is of exactly the same form as the equation solved by Glaser[7] for electron trajectories in a "bell-shaped" magnetic electron microscope lens field. A very simple solution exists, which treats the "thickness" of the lens exactly, and predicts focal lengths and principal

plane locations for both the immersion case (when the image and/or object is within the field of the lens) and the asymptotic case. The immersion case is particularly interesting for the donut mode laser-atomic lens because this is where the shortest focal lengths, and hence the smallest aberrations, occur. As will be discussed in Section 2, we find that the lens has a minimum focal length, reached when the focal spot is at the center of the lens and the focal length is equal to the Rayleigh length of the laser beam. This has important design consequences in that infinitely short focal lengths cannot be achieved. In addition, the optimum configuration for obtaining the minimum spot size (in the zero magnification case) is a symmetric arrangement with the focus at the center of the lens.

Having analytic expressions for the first order properties of the lens, accurate expressions for contributions to the spot size can be obtained. Aberrations can be treated exactly, without resorting to a thin lens approximation. We obtain analytic expressions for spherical and chromatic aberration, as well as compact expressions for the aberrations arising from both spontaneous emission and dipole force fluctuations. Diffraction of the atoms is treated as it would be in the case of geometric optics, i.e., Frauenhofer diffraction of the atom beam is assumed based on the de Broglie wavelength of the atoms and the angle of convergence of the beam at the focal spot. This is valid provided the potential does not change rapidly over the scale of an atomic wavelength, which is essentially the requirement for the WKB approximation. The effect on the spot diameter of a finite source size, or equivalently, an imperfectly collimated atom beam, is also very simply obtained knowing the focal length and principal plane location.

In Section 2, we discuss the solution of the first order paraxial equation of motion

for the atoms in the TEM_{01}^{*} laser field, and the resulting description of the lens in terms of cardinal elements. Section 3 covers spot size contributions. In Section 4, we discuss numerical examples, comparing our results to those of Gallatin and Gould,[6] and examining the case of optimum focusing with the shortest focal length. Optimization of the lens is covered in Section 5, where a practical formula for the net spot size is derived and minimized.

2 First order lens properties

2.1 Paraxial equation of motion

In this section we derive the first order equation of motion governing the focusing of a cylindrically symmetric atom beam in the TEM_{01}^{*} laser field. The optic axis, the axis of symmetry, is the z-axis, with $z = 0$ located at the center of the laser focus (minimum beam waist). The equation of motion can be derived from the Lagrangian, $L = (\dot{x}^2 + \dot{y}^2 + \dot{z}^2)/2m - U(r,z)$ in the standard way[8]. Here, $\dot{x}$ denotes the atom velocity along the x-axis, m is the atomic mass, and $U(r,z)$ is the potential energy. In cylindrical coordinates, assuming that the initial angular momentum about the z-axis is zero, the radial equation of motion simplifies to

$$\ddot{r} + \frac{1}{m}\frac{\partial U(r,z)}{\partial r} = 0. \tag{1}$$

The conservation of energy is used to parameterize this equation in terms of the distance along the optic axis, z. With this parameterization, the all-orders equation of motion becomes

$$\frac{d}{dz}\left[(1-\frac{U(r,z)}{E_o})^{1/2}(1+r'^2)^{-1/2}r'\right] + \frac{1}{2E_o}(1-\frac{U(r,z)}{E_o})^{-1/2}(1+r'^2)^{1/2}\frac{\partial U(r,z)}{\partial r} = 0. \tag{2}$$

Here, E_o is the incident atomic beam kinetic energy, and r' denotes differentiation of r with respect to z.

In order to solve eq. (2), we need the potential energy $U(r,z)$ of the atom in the laser field. The potential energy is given by[4]

$$U(r,z) = \frac{\hbar\Delta}{2}\ln\left[1 + p(r,z)\right], \tag{3}$$

where $\Delta = \omega - \omega_o$ is the laser detuning from the atomic resonant frequency. Here, ω

and ω_o are the laser and atomic resonance angular frequencies, and $p(r,z)$, the atomic transition saturation parameter, is given by

$$p(r,z) = \frac{I(r,z)}{I_s}\frac{\gamma^2}{\gamma^2 + 4\Delta^2}. \tag{4}$$

In the expression for $p(r,z)$, γ is the natural atomic resonance linewidth (in rad/s), I_s is the atomic saturation transition intensity, and $I(r,z)$ is the laser intensity distribution for the TEM_{01}^* donut mode, given by

$$I(r,z) = 8I_o\frac{w_o^2 r^2}{w^4(z)}\exp\left[-\frac{2L^2}{w_o^2}\frac{r^2}{L^2+z^2}\right]. \tag{5}$$

The parameter w_o determines the radius of the laser beam at the waist; the peak intensity is found at a distance $w_o/\sqrt{2}$ from the axis. The quantity L is the Rayleigh length, given by $L = \pi w_o^2/\lambda$, λ is the laser wavelength, $w^2(z) = w_o^2(1+z^2/L^2)$, and I_o is the laser intensity at the beam waist, related to the laser power P_o by $I_o = P_o/2\pi w_o^2$.

The first order solution of eq. (2) involves making the assumptions that $U(r,z) \ll E_o$ and $r' \ll 1$. The equation then simplifies to

$$r'' + \frac{1}{2E_o}\frac{\partial U(r,z)}{\partial r} = 0. \tag{6}$$

We then expand the potential in r around the z-axis. This expansion involves both the exponential in the expression for the laser beam intensity, and also the logarithm in the expression for the potential. In order for this to be a valid expansion, we require $r^2 \ll w_o^2$ and $p(r,z) \ll 1$. Taking into account the first of these requirements, the second becomes $p_o = \mathcal{O}(1)$, where p_o is the space-independent part of $p(r,z)$:

$$p_o = 8\frac{\gamma^2}{\gamma^2+4\Delta^2}\frac{I_o}{I_s}. \tag{7}$$

Expanding the potential, we find that the lowest order term is quadratic in r:

$$U_2(r,z) = \frac{\hbar\Delta p_o w_o^2}{2w^4(z)}r^2. \tag{8}$$

We note, as pointed out by Balykin and Letokhov,[5] that this quadratic dependence on r provides the necessary radial dependence of the potential for a Newtonian lens description. Inserting eq. (8) into eq. (6) results in the first order paraxial equation of motion

$$r'' + p_o \frac{\hbar\Delta}{2E_o} \frac{w_o^2}{w^4(z)} r = 0. \tag{9}$$

At this point, we introduce the excitation parameters k and q, and rewrite the equation of motion in dimensionless form. The excitation parameters are

$$k^2 = p_o \frac{\hbar\Delta}{2E_o} \frac{L^2}{w_o^2} \tag{10}$$

and

$$q^2 = k^2 + 1. \tag{11}$$

The dimensionless variables are $R = r/L$ and $Z = z/L$. With these substitutions, the first order equation of motion (9) can be written in the simple dimensionless form

$$R'' + \frac{k^2}{(1+Z^2)^2} R = 0. \tag{12}$$

This differential equation can be cast in a form where an analytic solution exists, first developed by Glaser[7], by making the substitution $Z = -\cot\phi$. We note that $\phi = 0$ at $z = -\infty$ and $\phi = \pi$ at $z = +\infty$ (see Fig. 2). With this substitution, the equation of motion becomes

$$R'' + 2\cot\phi R' + k^2 R = 0 \tag{13}$$

(primes now indicate differentiation with respect to ϕ). A further substitution of $R(\phi) = y(\phi)/\sin\phi$ results in the simple differential equation

$$y'' + q^2 y = 0. \tag{14}$$

The general solution to eq. (14) is a linear combination of $\sin q\phi$ and $\cos q\phi$, which can be converted into a general expression for the dimensionless trajectory

$$R(\phi) = \frac{1}{\sin\phi}\left(c_1 \sin q\phi + c_2 \cos q\phi\right), \tag{15}$$

where c_1 and c_2 are constants chosen to specify the trajectory of interest. For example, a ray moving in the positive z direction initially parallel to the z-axis at a distance r_o is described by the trajectory

$$R(\phi) = \frac{r_o}{L}\frac{\sin q\phi}{q \sin\phi}. \tag{16}$$

This trajectory is particularly useful in determining the cardinal elements of the lens; an example is shown in Fig. 2.

2.2 Cardinal elements

Since the first order paraxial equation for the donut mode laser-atomic lens is identical to the equation treated by Glaser in his "bell"-shaped magnetic lens field model, we can extract all the first order properties of the lens from his work. The lens has the following important characteristics. (a) It is a thick lens, and hence its cardinal elements include both principal planes and focal lengths, instead of only a single focal length. (b) It is a symmetric lens, so principal planes and focal spots for the image side and object side are located at equal distances from the lens center. (c) For sufficiently large excitation, the lens can have multiple crossovers. (d) For all image and object plane locations, even in the immersion case, the lens is still Newtonian in the sense that the simple Newtonian lens law applies for determining magnification, image locations, etc., in terms of the cardinal elements of the lens.

The image-side focal point of the lens is determined by considering the initially parallel trajectory described by eq. (16). A focal point exists for the values of ϕ

$(0 < \phi < \pi)$ which result in $R(\phi) = 0$. This occurs when $\phi = n\pi/q$, where n is an integer between 1 and the largest integer less than q. Thus the image-side focal points are given by

$$z_f = L\cot(\frac{n\pi}{q}). \tag{17}$$

We see that for $1 \leq q \leq 2$, the lens has a single focal point ranging in location from $z = +\infty$ to $z = 0$. The principal plane locations and focal lengths are determined from the trajectory of eq. (16) as shown in Fig. 2. Using eq. (16), we obtain the image side principal plane locations

$$z_p = \begin{cases} -L\cot(\frac{n\pi}{2q}) & (n \text{ odd}) \\ L\tan(\frac{n\pi}{2q}) & (n \text{ even}), \end{cases} \tag{18}$$

and the focal lengths

$$f = (-1)^{n+1}\frac{L}{\sin(n\pi/q)}. \tag{19}$$

The linear and angular magnifications, M and m, are given by

$$M = \frac{1}{m} = (-1)^n\frac{\sin\phi_o}{\sin\phi_i}, \tag{20}$$

where ϕ_o and ϕ_i are the values of ϕ corresponding to the object and image positions. We note that, though not required for a treatment in terms of cardinal elements, the lens behavior is simplest when the number of focal points is kept to one. Hence the expressions (17-20) are generally used with $n = 1$.

Fig. 3 shows the behavior of the focal length f and the principal plane location z_p as a function of lens excitation q. Several interesting features of the lens become apparent on examining these curves. For example, all the first order properties of the lens are determined by a single parameter q, given by eqs. (10-11). This makes characterization of the lens simple, and shows that, at least to first order, there are

many combinations of incident atomic velocity, laser power, detuning, and laser beam waist w_o which result in identical lens behavior.

Furthermore, as seen in Fig. 3, the focal length goes through a minimum, reached when $q = 2$. Thus the lens does not become infinitely strong focusing as the excitation is increased, as might be expected. Instead, for $q > 2$, the principal plane moves in the negative z-direction faster than the focal point as a function of excitation, resulting in a longer focal length. The shortest focal length occurs when $f = L$ and $z_p = -L$, i.e., the focal point is at the center of the lens. This is sometimes referred to as the "telescopic" mode of focusing, because the trajectory enters and leaves the lens parallel to the z-axis. The minimum focal length condition has important implications when considering the optimization of the lens, as this is generally a configuration in which diffraction and some aberrations are minimized.

3 Spot size limitations

The determination of the ultimate spot size for an initially (nearly) parallel atom beam brought to a focus at the focal point of the lens is of central importance in the analysis of the donut mode laser-atomic lens. We consider the contributions of aberrations, as well as the effects of diffraction and a finite source size (i.e., an imperfectly collimated atom beam). The aberrations include spherical aberration, chromatic aberration, and two "diffusive" aberrations, one resulting from spontaneous emission and the other from dipole force fluctuations. In each case, the ultimate result is an expression for the full width at half maximum (FWHM) spot diameter of the beam at the focus in terms of laser and atom beam parameters. To obtain the net spot size, we add all contributions in quadrature.

3.1 Aberrations

Due to the simple analytic nature of the paraxial solutions to the ray equation, it is possible to do a fairly rigorous treatment of the aberrations. Though the immediate interest is in the spot size at the focus for an initially parallel beam, we obtain expressions for the aberrations in the general case of finite object and image distances. These will prove useful in cases where the lens is used for imaging. We then consider the limiting case of zero magnification (i.e., object at $-\infty$, image at the focal point), and obtain expressions for the FWHM spot diameters. All the aberrations of the lens are treated with essentially the same method, in which a (small) deviation ε from the paraxial trajectory is calculated. The method is described in several texts on electron optics.[9, 10, 11] For each aberration, a differential equation for the deviation ε is arrived at, which is the same as the paraxial equation (eq. 12), with an additional

inhomogeneous term on the right hand side. This inhomogeneous differential equation is solved by the method of variation of parameters.[12] The method involves choosing two linearly independent solutions to eq. (12), $R_1(Z)$ and $R_2(Z)$. If we choose $R_1(Z)$ such that it equals zero at the image plane ($Z = Z_i$), the deviation in R_1 at the image plane due to an aberration can be expressed in terms of the following integral (see e.g. Ref. [9]):

$$\varepsilon = \frac{R_2(Z_i)}{R_1 R_2' - R_1' R_2} \int_{Z_o}^{Z_i} R_1(Z) W(R_1, R_1', Z) dZ, \tag{21}$$

where $W(R_1, R_1', Z)$ is the inhomogeneous term in the differential equation. The quantity $R_1 R_2' - R_1' R_2$ is the Wronskian of the two solutions R_1 and R_2, which is a constant due to their linear independence.

In the general case, when the object and image planes are both at finite distances from the lens, it is most useful to define aberration coefficients, which are used for determining the trajectory error at the image plane for a trajectory R_1 which originates on the axis at the object with a slope α_o. This trajectory, shown in Fig. 4, also crosses the axis at the image plane, making an angle $\alpha_i = \alpha_o/|M|$, where M is the linear magnification of the lens. Following electron-optical conventions, we define spherical, chromatic, spontaneous emission and dipole fluctuation aberration coefficients $C^o_{\rm sph}, C^o_{\rm chr}, C^o_{\rm spont}$, and $C^o_{\rm dip}$, referred to the object plane, by the following relations:

$$|\varepsilon_{\rm sph}| = |M| \alpha_o^3 \frac{C^o_{\rm sph}}{L} \tag{22}$$

$$|\varepsilon_{\rm chr}| = |M| \alpha_o \epsilon \frac{C^o_{\rm chr}}{L} \tag{23}$$

$$\varepsilon_{\rm spont} = |M| \alpha_o \frac{C^o_{\rm spont}}{L} \tag{24}$$

$$\varepsilon_{\rm dip} = |M| \alpha_o^3 \frac{C^o_{\rm dip}}{L}, \tag{25}$$

where ϵ is a fractional deviation in the energy of the atom beam, to be discussed below. Absolute values of ε and M are taken so that the aberration coefficients can be related to spot diameters. The powers of α_o used in these definitions are chosen to remove any α_o dependence from the coefficients themselves. That the correct power has been chosen for each aberration will become clear below. Since the spontaneous and dipole aberrations are diffusive in nature, the quantities $\varepsilon_{\text{spont}}$ and ε_{dip} are interpreted as RMS values.

To determine the aberration coefficients, we require an explicit expression for the ray R_1. For convenience, we characterize the trajectories in terms of the variable $\phi = \arctan Z + \pi/2$, instead of Z, and use solutions of the form shown in eq. (15). We write $R_1(\phi) = \alpha_o h(\phi)$, where

$$h(\phi) = \frac{\sin\left[q(\phi - \phi_o)\right]}{q \sin\phi \sin\phi_o}. \tag{26}$$

For R_2, we choose an independent solution which has the property $R_2(\phi_o) = 1$, so that at the image plane, $R_2(\phi_i) = M$. Though we do not need the explicit form of R_2, we note that it is

$$R_2(\phi) = g(\phi) = \frac{\sin\phi_o}{\sin\phi} \frac{\sin\left[q(\phi - \alpha)\right]}{\sin\left[q(\phi_o - \alpha)\right]}, \tag{27}$$

where $\alpha = \phi_o - \frac{1}{q}\tan^{-1}(q \tan\phi_o)$. The trajectories $h(\phi)$ and $g(\phi)$ are the standard trajectories used for aberration analysis in electron optics.[10]

With this choice of R_1 and R_2, the denominator in eq. (21) becomes $-\alpha_o$, and we can write

$$\varepsilon = -M \int_{\phi_o}^{\phi_i} h(\phi) W(\alpha_o h, \alpha_o h', \phi) \frac{dZ}{d\phi} d\phi. \tag{28}$$

Using eqs. (22) and (23), we can now write

$$C^o_{\text{sph}} = \left| \frac{L}{\alpha_o^3} \int_{\phi_o}^{\phi_i} h(\phi) W_{\text{sph}}(\alpha_o h, \alpha_o h', \phi) \frac{d\phi}{\sin^2\phi} \right| \tag{29}$$

$$C^o_{\rm chr} = \left| \frac{L}{\alpha_o \epsilon} \int_{\phi_o}^{\phi_i} h(\phi) W_{\rm chr}(\alpha_o h, \alpha_o h', \phi) \frac{d\phi}{\sin^2 \phi} \right|. \tag{30}$$

The expressions for the diffusive aberration coefficients $C^o_{\rm spont}$ and $C^o_{\rm dip}$ are similar to eqs. (29) and (30), though a little more complicated due to the random nature of the forces involved. They will be discussed in more detail below.

The determination of the aberration coefficients is now reduced to finding the inhomogeneous terms for each aberration source and carrying out the integral in eqs. (29) and (30).

3.1.1 Spherical aberration

Spherical aberration arises when higher order terms in the expansion of the equation of motion are not neglected. This is a manifestation of the fact that for large enough r, the potential is no longer simply quadratic in r. Since the potential is cylindrically symmetric, the next higher term is proportional to r^4. The equation of motion depends on $\partial U/\partial r$, so its next higher term is of order r^3. To correctly include all terms in r^3, we must keep contributions from the expansion of the all-orders equation of motion (eq. 2) as well as contributions from the expansion of the potential. The resulting third order inhomogeneous term is

$$\begin{aligned} W_{\rm sph}(R, R', Z) \;=\; & k^2 R^3 \left[\left(p_o \frac{L^2}{w_o^2} - k^2 \right) \frac{1}{(1+Z^2)^4} + 4 \frac{L^2}{w_o^2} \frac{1}{(1+Z^2)^3} \right] \\ & - k^2 R^2 R' \left[\frac{2Z}{(1+Z^2)^3} \right] - k^2 R R'^2 \left[\frac{1}{(1+Z^2)^2} \right]. \end{aligned} \tag{31}$$

Converting Z to ϕ and R to $\alpha_o h(\phi)$, we can insert eq (31) into eq. (29) to obtain an explicit integral for the spherical aberration coefficient:

$$C^o_{\rm sph} = \left| \frac{k^2 L}{q^4 \sin^4 \phi_o} \left[p_o \frac{L^2}{w_o^2} + 4 \right] \int_{\phi_o}^{\phi_i} \sin^2 \phi \sin^4 \left[q(\phi - \phi_o) \right] d\phi \right.$$

$$+\frac{k^2 L}{q^4 \sin^4\phi_o}\left[4\frac{L^2}{w_o^2}-3\right]\int_{\phi_o}^{\phi_i}\sin^4\left[q(\phi-\phi_o)\right]d\phi$$

$$-\frac{k^2 L}{q^2 \sin^4\phi_o}\int_{\phi_o}^{\phi_i}\sin^2\phi\sin^2\left[q(\phi-\phi_o)\right]d\phi$$

$$+\frac{4k^2 L}{q^3 \sin^4\phi_o}\int_{\phi_o}^{\phi_i}\sin\phi\cos\phi\cos\left[q(\phi-\phi_o)\right]\sin^3\left[q(\phi-\phi_o)\right]d\phi\Bigg|. \qquad (33)$$

All the integrals in eq. (33) can be done analytically, and the resulting spherical aberration coefficient referred to the object plane is given by

$$C_{\rm sph}^o = \frac{L}{\sin^4\phi_o}\frac{3\pi k^2}{8q^5}\left[\frac{L^2}{2w_o^2}(p_o+8)-\frac{5+2k^2}{3}\right]$$

$$-\frac{L}{\sin^4\phi_o}\frac{1}{8(4k^2+3)}\left[3p_o\frac{L^2}{w_o^2}+15-4k^2\right]\left(\sin(2\phi_o+\frac{2\pi}{q})-\sin(2\phi_o)\right). \qquad (34)$$

In going from eq. (33) to eq. (34), we have made use of the object-image relation

$$\phi_i = \phi_o + \frac{n\pi}{q}, \qquad (35)$$

obtained from finding the zeros of $h(\phi)$. In addition, we have restricted ourselves to the case where $n = 1$, so eq. (34) is valid only for the first image in a multiple crossover lens. The absolute value has been dropped because the sign of $C_{\rm sph}^o$ can be shown to remain unchanged fro all excitations.[9]

The spherical aberration coefficient given in eq. (34) can be used in this form for any situation in which the object and image positions are finite. However, it is often convenient to expand the coefficient as a polynomial in $1/M$. This is useful if the main design consideration of a lens is the magnification, or if M is particularly large or small. It can be shown[10, 11] that $C_{\rm sph}^o$ can be uniquely represented by a fourth order polynomial, i.e.,

$$C_{\rm sph}^o = C_{\rm sph0}^o + \frac{C_{\rm sph1}^o}{M} + \frac{C_{\rm sph2}^o}{M^2} + \frac{C_{\rm sph3}^o}{M^3} + \frac{C_{\rm sph4}^o}{M^4}. \qquad (36)$$

The coefficients of the polynomial can be extracted from eq. (34) via the relationship

$$-\cot\phi_o = \frac{1}{M\sin(\pi/q)} + \cot(\pi/q), \tag{37}$$

derived from the expression for the magnification eq. (20) and the object-image relation eq. (35). Substituting eq. (37) into eq. (34), we get the polynomial coefficients

$$C^o_{\text{sph0}} = C^o_{\text{sph4}} = \frac{3\pi k^2 L}{8q^5\sin^4(\pi/q)}\left[\frac{L^2}{2w_o^2}(p_o+8) - \frac{5+2k^2}{3}\right] - \frac{L\sin(2\pi/q)}{8(4k^2+3)\sin^4(\pi/q)}\left[3p_o\frac{L^2}{w_o^2} + 15 - 4k^2\right] \tag{38}$$

$$C^o_{\text{sph1}} = C^o_{\text{sph3}} = \frac{3\pi k^2 L\cos(\pi/q)}{2q^5\sin^4(\pi/q)}\left[\frac{L^2}{2w_o^2}(p_o+8) - \frac{5+2k^2}{3}\right] - \frac{L\,[3+\cos(2\pi/q)]}{4(4k^2+3)\sin^3(\pi/q)}\left[3p_o\frac{L^2}{w_o^2} + 15 - 4k^2\right] \tag{39}$$

$$C^o_{\text{sph2}} = \frac{3\pi k^2 L\,[2+\cos(2\pi/q)]}{4q^5\sin^4(\pi/q)}\left[\frac{L^2}{2w_o^2}(p_o+8) - \frac{5+2k^2}{3}\right] - \frac{3L\cos(\pi/q)}{2(4k^2+3)\sin^3(\pi/q)}\left[3p_o\frac{L^2}{w_o^2} + 15 - 4k^2\right] \tag{40}$$

The expression for C^o_{sph} in terms of M is very useful for most imaging situations, because the coefficients need only be calculated once and the spherical aberration is known for all object-image distances. However, it poses a slight problem when we wish to consider the zero magnification ("parallel-in") case because C^o_{sph} becomes infinite, while α_o goes to zero. The spot size, of course, does not become infinite. The way around this awkwardness is to use the spherical aberration coefficient C^i_{sph} defined in terms of the trajectory angle α_i at the image plane. We write

$$|\varepsilon_{\text{sph}}| = \alpha_i^3\frac{C^i_{\text{sph}}}{L}, \tag{41}$$

which then requires that

$$C^i_{\text{sph}} = M^4 C^o_{\text{sph}}, \tag{42}$$

where we have used the fact that $\alpha_i = \alpha_o/|M|$. Using eqs. (42) and (36), we find that

$$C^i_{\rm sph}(M=0) = C^o_{\rm sph4}. \tag{43}$$

Eq. (41) can now be used to obtain the spot size for the zero magnification case. To obtain the minimum spot size, we note that the diameter can be taken at the circle of least confusion, at which point the FWHM spot size $\delta_{\rm sph}$ is given by $\frac{1}{2}L|\varepsilon_{\rm sph}|$. For a ray incident at a radius r_o, the angle at the image plane is given by

$$\alpha_i = \frac{r_o}{f} = \frac{r_o}{L}\sin(\pi/q). \tag{44}$$

The final expression for the spot size due to spherical aberration at the circle of least confusion then becomes

$$\begin{aligned}\delta_{\rm sph} = &\frac{3\pi k^2 r_o^3}{16L^2q^5\sin(\pi/q)}\left[\frac{L^2}{2w_o^2}(p_o+8) - \frac{5+2k^2}{3}\right] \\ &- \frac{r_o^3\cos(\pi/q)}{8L^2(4k^2+3)}\left[3p_o\frac{L^2}{w_o^2} + 15 - 4k^2\right]\end{aligned} \tag{45}$$

3.1.2 Chromatic aberration

Chromatic aberration arises from a finite energy spread in the incident atom beam. Atoms with different initial kinetic energies follow different trajectories through the lens, resulting in a smearing out of the focal spot.

The chromatic aberration coefficient can be calculated in an analogous way to the spherical aberration. The energy E_o in the paraxial equation (9) must be replaced by $E_o(1+\epsilon)$, where ϵ is a fractional energy deviation. When the equation is expanded and the lowest order terms retained, the following differential equation results:

$$r'' + \frac{\hbar\Delta p_o}{2E_o}\frac{w_o^2}{w^4(z)}r = \epsilon\frac{\hbar\Delta p_o}{2E_o}\frac{w_o^2}{w^4(z)}r \tag{46}$$

We see that the inhomogeneous term in this case is

$$W_{\rm chr}(R, R', Z) = \frac{k^2}{(1+Z^2)^2}\epsilon R, \tag{47}$$

where conversion to dimensionless variables has been carried out. Substituting this into eq. (30) and using the object-image relation eq. (35) yields the chromatic aberration coefficient

$$C^o_{\rm chr} = \frac{\pi k^2 L}{2q^3 \sin^2\phi_o}. \tag{48}$$

Eq. (48) is an exact expression for the chromatic aberration coefficient in the finite object-image case. As with spherical aberration, it is useful to write it in terms of a polynomial in the linear magnification M. In this case, it is only necessary to include powers up to M^{-2}:

$$C^o_{\rm chr} = C^o_{\rm chr0} + \frac{C^o_{\rm chr1}}{M} + \frac{C^o_{\rm chr2}}{M^2}. \tag{49}$$

The expansion coefficients are given by

$$C^o_{\rm chr0} = C^o_{\rm chr2} = -\frac{\pi k^2 L}{2q^3}\frac{1}{\sin^2(\pi/q)} \tag{50}$$

$$C^o_{\rm chr1} = -\frac{\pi k^2 L}{q^3}\frac{\cos(\pi/q)}{\sin^2(\pi/q)} \tag{51}$$

Converting to the image plane chromatic aberration coefficient, defined by

$$|\varepsilon_{\rm chr}| = \alpha_i \epsilon \frac{C^i_{\rm chr}}{L}, \tag{52}$$

we obtain

$$C^i_{\rm chr} = M^2 C^o_{\rm chr}, \tag{53}$$

from which we arrive at the FWHM spot diameter for the zero magnification case

$$\delta_{\rm chr} = \frac{\pi k^2 r_o}{2q^3 \sin(\pi/q)}\frac{\Delta E_{1/2}}{E_o}, \tag{54}$$

where $\Delta E_{1/2}$ is the FWHM of the energy distribution of the atom beam.

3.1.3 "Diffusive" aberrations

Since the spontaneous and dipole aberrations are the result of random forces, the average deviation along a particle trajectory is zero. The deviations from the paraxial trajectories must therefore be treated in terms of RMS values. The formalism for this resembles the treatment of Brownian motion[13]. We consider the radial equation of motion eq. (1) with an additional inhomogeneous force term on the right hand side:

$$\ddot{r} + \frac{1}{m}\frac{\partial U(r,z)}{\partial r} = \frac{1}{m}F_r(t). \tag{55}$$

$F_r(t)$ is a random force for which $< F_r(t) >= 0$, but $< F_r(t)F_r(t') > \neq 0$. Converting eq. (55) to a paraxial form, we make the approximation $z \approx v_o t$, where $v_o = \sqrt{2E_o/m}$ is the initial atomic velocity, and write

$$r'' + \frac{1}{2E_o}\frac{\partial U(r,z)}{\partial r} = \frac{1}{2E_o}F_r(\frac{z}{v_o}). \tag{56}$$

Converting to dimensionless variables, we can make the association

$$W(R,R',Z) = \frac{L}{2E_o}F_r(\frac{LZ}{v_o}). \tag{57}$$

This allows us to write down an expression for the mean-squared trajectory deviation similar to eq. (21), though containing a double integral to account for the random nature of W. To simplify the following expressions, we suppress the explicit R and R' dependence in W, writing only $W(Z)$ and bearing in mind that some of the Z-dependence may come through an R- or R'-dependence. We get

$$< \varepsilon^2 >= \frac{R_2(Z_i)^2}{(R_1R_2' - R_1'R_2)^2}\int_{Z_o}^{Z_i} dZ \int_{Z_o}^{Z_i} dZ' R_1(Z)R_1(Z') < W(Z)W(Z') > . \tag{58}$$

Putting, as before, the solution $R_1 = \alpha_o h(\phi)$ into eq. (58) and changing variables from Z to ϕ, we obtain expressions for the spontaneous and dipole aberration coefficients

$$C^o_{\text{spont}} = \frac{L}{\alpha_o}\left[\int_{\phi_o}^{\phi_i}\frac{d\phi}{\sin^2\phi}\int_{\phi_o}^{\phi_i}\frac{d\phi'}{\sin^2\phi'}h(\phi)h(\phi') < W_{\text{spont}}(\phi)W_{\text{spont}}(\phi') >\right]^{1/2} \tag{59}$$

$$C^o_{\rm dip} = \frac{L}{\alpha_o^3}\left[\int_{\phi_o}^{\phi_i}\frac{d\phi}{\sin^2\phi}\int_{\phi_o}^{\phi_i}\frac{d\phi'}{\sin^2\phi'}h(\phi)h(\phi') < W_{\rm dip}(\phi)W_{\rm dip}(\phi') >\right]^{1/2} \qquad (60)$$

In order to make use of eqs. (59) and (60), we must now determine the autocorrelations of the inhomogeneous terms $W_{\rm spont}$ and $W_{\rm dip}$.

The spontaneous emission aberration arises as a result of the random momentum changes of size h/λ which occur each time a photon is spontaneously emitted. The average rate at which these changes occur depends on the intensity of the laser, and, for low intensities, it equals $\gamma p/2$, where γ is the natural linewidth of the atomic transition in rad/s, and p is the saturation parameter given in eq. (4).[4] Over the time scale of interest, i.e., the time over which the focusing potential changes as the atom passes through the lens, the momentum changes can be considered as occurring over an infinitely short time, and to be completely uncorrelated. With this assumption, we can write

$$< F_{\rm spont}(t)F_{\rm spont}(t') >= \frac{2}{3}\gamma\frac{p(r,z)}{2}\left(\frac{h}{\lambda}\right)^2\delta(t-t'). \qquad (61)$$

The factor of $\frac{2}{3}$ is a result of averaging over two of the three spatial degrees of freedom in the spontaneous emission process. Assuming paraxial conditions, the saturation parameter $p(r,z)$ can be written in terms of ϕ as

$$p(r,z) \approx p_o\frac{L^2}{w_o^2}\frac{R^2}{(1+Z^2)^2} = p_o\frac{L^2}{w_o^2}R^2(\phi)\sin^4\phi. \qquad (62)$$

Combining eqs. (57), (61) and (62), we can deduce

$$< W_{\rm spont}(\phi)W_{\rm spont}(\phi') >= \frac{L^3h^2v_o\gamma p_o}{12w_o^2E_o^2\lambda^2}R^2(\phi)\sin^6\phi\,\delta(\phi-\phi'), \qquad (63)$$

where we have made use of the fact that $\delta(Z-Z') = \sin^2\phi\,\delta(\phi-\phi')$. Inserting eq. (63) for the autocorrelation of the spontaneous emission inhomogeneous term into

the expression (eq. 59) for the aberration coefficient and substituting $R(\phi) = \alpha_o h(\phi)$, we obtain

$$C^o_{\text{spont}} = \frac{L^2 h}{\lambda w_o E_o}\left[\frac{L v_o \gamma p_o}{12}\int_{\phi_o}^{\phi_i} h^4(\phi)\sin^2\phi d\phi\right]^{1/2} \tag{64}$$

Putting in the definition of $h(\phi)$ (eq. 26), we get

$$C^o_{\text{spont}} = \frac{L^2 h}{\lambda w_o E_o}\left(\frac{L v_o \gamma p_o}{12}\right)^{1/2}\frac{1}{q^2\sin^2\phi_o}\left[\int_{\phi_o}^{\phi_i}\frac{\sin^4[q(\phi-\phi_o)]}{\sin^2\phi}\right]^{1/2}. \tag{65}$$

The integral in eq. (65) is not analytic, so a numerical evaluation of this equation must be used to obtain the aberration coefficient. In addition, the convenient expansion into a polynomial in the magnification is not possible. Nevertheless, the expression is still useful when one is interested in the aberration coefficient for the finite magnification case.

Since the magnification expansion is not possible, and hence we cannot easily convert to the aberration coefficient referred to the image plane, another approach must be taken to obtain the spot size for the zero magnification case. Instead of letting $R_1 = \alpha_o h(\phi)$ in eq. (58), we can use the "parallel-in" trajectory of eq. (16), since the choice of solutions in the variation of parameters method is arbitrary. We note that this trajectory crosses the axis at the focus, so eq. (58) is still valid. A linearly independent solution is needed for R_2, for which we use

$$R_2 = -\sin(\pi/q)\frac{\cos(q\phi)}{\sin\phi}, \tag{66}$$

We note that $R_2 = 1$ at the focus ($\phi = \pi/q$). The Wronskian of R_1 and R_2 is now $-(r_o/L)\sin(\pi/q)$, and we can write

$$<\varepsilon^2> = \frac{L^2}{r_o^2\sin^2(\pi/q)}\int_0^{\pi/q}\frac{d\phi}{\sin^2\phi}\int_0^{\pi/q}\frac{d\phi'}{\sin^2\phi'}R_1(\phi)R_1(\phi')<W(\phi)W(\phi')> \tag{67}$$

Putting eqs. (63) and (16) into this expression leads to an expression for the zero magnification aberration coefficient referred to the image plane (defined by $\varepsilon_{\rm spont} = |\alpha_i| C^i_{\rm spont}/L$):

$$C^i_{\rm spont}(M=0) = \frac{L}{q^2 \sin^2(\pi/q)} \left(\frac{L^3 h^2 v_o \gamma p_o}{12 w_o^2 E_o^2 \lambda^2} \right)^{1/2} \left[\int_0^{\pi/q} \frac{\sin^4 q\phi}{\sin^2 \phi} d\phi \right]^{1/2}, \qquad (68)$$

where we have made use of the fact that $\alpha_i = r_o/f = r_o \sin(\pi/q)/L$. The FWHM spot diameter follows immediately from this, i.e.,

$$\delta_{\rm spont} = 2\sqrt{2\ln 2} \frac{r_o}{q^2 \sin(\pi/q)} \left(\frac{L^3 h^2 v_o \gamma p_o}{12 w_o^2 E_o^2 \lambda^2} \right)^{1/2} \left[\int_0^{\pi/q} \frac{\sin^4 q\phi}{\sin^2 \phi} d\phi \right]^{1/2}, \qquad (69)$$

where the factor of $2\sqrt{2\ln 2}$ provides the conversion from RMS to FWHM.

The dipole fluctuation aberration is treated in an identical manner to the spontaneous emission aberration. As has been discussed by Dalibard and Cohen-Tannoudji,[14] the dipole force can reverse sign temporarily each time a photon is spontaneously emitted. The fluctuating part of the dipole force which results from this random sign change can be considered as an inhomogeneous driving term $F_r(t)$ in the equation of motion, for which $< F_r(t) >= 0$ but $< F_r(t) F_r(t') > \neq 0$, just as with spontaneous emission. For small saturation parameters $p \ll 1$, the autocorrelation of the fluctuating part of the dipole force can be written as[14]

$$< F_{\rm dip}(t) F_{\rm dip}(t') >= \frac{\hbar^2 \Delta^2}{4} (\nabla p)^2 p^2 e^{-\gamma |t-t'|}. \qquad (70)$$

Using the expression in eq. (62) for the saturation parameter in the donut mode laser-atomic lens, letting $\nabla \rightarrow \partial/\partial r$, and converting t to LZ/v_o as before, we can write

$$< W_{\rm dip}(Z) W_{\rm dip}(Z') >= k^4 p_o^2 \frac{L^4}{w_o^4} \frac{R^6(Z)}{(1+Z^2)^8} e^{-\frac{\gamma L}{v_o}|Z-Z'|}. \qquad (71)$$

This expression leads to a very complicated integral when conversion is made to the variable ϕ for calculating the aberration coefficient. It suffices at present to consider the limit $\gamma L/v_o \gg 1$, which occurs when the number of spontaneous emissions is large during transit through the lens. The approximation should be good because the aberration itself is only significant when a large number of spontaneous emission events take place. In this limit, we can say

$$e^{-\frac{\gamma L}{v_o}|Z-Z'|} \approx \frac{2v_o}{\gamma L}\delta(Z-Z') \tag{72}$$

We can now write down an approximate autocorrelation in ϕ of the inhomogeneous term in the differential equation

$$< W_{\rm dip}(\phi)W_{\rm dip}(\phi') >= 2\frac{v_o}{\gamma L}k^4 p_o^2 \frac{L^4}{w_o^4} R^6(\phi)\sin^{18}\phi\,\delta(\phi-\phi') \tag{73}$$

This can be inserted into eq. (60) to obtain the dipole fluctuation aberration coefficient

$$C^o_{\rm dip} = \frac{L^3}{w_o^2}\left(\frac{2v_o}{\gamma L}\right)^{1/2}\frac{k^2 p_o}{q^4\sin^4\phi_o}\left[\int_{\phi_o}^{\phi_i}\sin^6\phi\sin^8\left[q(\phi-\phi_o)\right]d\phi\right]^{1/2}. \tag{74}$$

The integral in eq. (74) is analytic, but extremely cumbersome. Therefore, as with the spontaneous aberration, we do not perform the expansion in magnification, but rather leave the expression for the aberration coefficient as is for use in the finite magnification case. For the zero magnification case, we proceed as we did with the spontaneous aberration, making use of the "parallel-in" trajectory for R_1 in eq. (58). Using eq. (67) with eq. (73) gives a zero magnification aberration coefficient referred to the image plane of

$$C^i_{\rm dip}(M=0) = \frac{L^3}{w_o^2}\left(\frac{2v_o}{\gamma L}\right)^{1/2}\frac{k^2 p_o}{q^4\sin^4(\pi/q)}\left[\int_0^{\pi/q}\sin^6\phi\sin^8 q\phi\; d\phi\right]^{1/2}, \tag{75}$$

and a FWHM spot diameter of

$$\delta_{\rm dip} = 4\sqrt{\ln 2}\frac{r_o^3}{w_o^2}\left(\frac{v_o}{\gamma L}\right)^{1/2}\frac{k^2 p_o}{q^4\sin(\pi/q)}\left[\int_0^{\pi/q}\sin^6\phi\sin^8 q\phi\; d\phi\right]^{1/2}. \tag{76}$$

3.2 Diffraction

The treatment of diffraction is straightforward once the paraxial trajectories are known. Since the potential in the lens is slowly varying as a function of z on the scale of the de Broglie wavelength $\lambda_{\rm dB}$ of the atom, we may apply thw WKB approximation, and make a complete analogy with the way diffraction is treated in ordinary geometric light optics. For a given initial intensity distribution in the atom beam, the final spot size can be determined from knowledge of the trajectories in exactly the same manner as it would be for a light beam. For instance, a diffraction-limited Gaussian atomic beam with a given waist radius and location can be propagated through the lens with the ray transfer ("ABCD") matrix derived from the principal plane locations and focal lengths. The spot size and location can be inferred from the radius of curvature and beam radius after the lens. Since the lens is Newtonian in the immersion case as well as in the asymptotic case, this approach is valid even when the focal spot is inside the lens.

Alternatively, one can assume the atom beam has a constant, circular intensity distribution formed by real apertures. In this case ordinary Frauenhofer diffraction is the appropriate optical analogy, and we obtain a simple expression for the FWHM of the diffracted intensity distribution at the image plane:

$$\delta_{\rm diffr} = \frac{0.61\lambda_{\rm dB}}{\alpha_i}, \tag{77}$$

For a beam initially parallel to the z-axis with radius r_o, α_i is given by r_o/f, where f is the focal length of the lens. Thus the FWHM spot diameter at the focus is

$$\delta_{\rm diffr} = \frac{0.61\lambda_{\rm dB}L}{r_o \sin(\pi/q)} \tag{78}$$

3.3 Finite source size

A perfectly parallel beam can be considered as arising from an infinitesimal source at $z = -\infty$. Of course, any real experiment has a finite source, or object, size d_o and a finite object distance z_o. This means that the focal spot will contain an image of the source, reduced in size by the magnification $M = z_i/z_o$. For very large z_o, $z_i \approx f$, and we can write the FWHM contribution to the spot diameter as

$$\delta_{\text{source}} = |M| d_o \approx \frac{f}{|z_o|} d_o, \tag{79}$$

where d_o is the FWHM of the source.

3.4 Net spot size at the focus

Rigorously speaking, it is not possible to predict the net spot size from separate calculations of the individual contributions. The aberrations in general interact with each other, and with the diffraction and source size effects. Furthermore, in practice, the net spot size is generally desired at the empirically determined position of smallest focus. This can be located at the focal plane, the circle of least confusion, or somewhere in between, depending on the relative sizes of the spot size contributions. Nevertheless, an overall sense of the magnitude of the net spot size can be obtained by combining the various contributions in quadrature. In analysis of a scanning transmission electron microscope (STEM) column, this approximation has been demonstrated to give the FWHM spot diameter within 10 percent of the true FWHM as determined by a full wave optical treatment.[15] The types of aberrations, their relative sizes, and the other spot size contributions in the STEM are similar to what is expected for a donut mode laser-atomic lens, so we can assume that the

approximation is appropriate in our case as well. Thus, as a general, but not precise, measure of the FWHM net spot diameter, we write

$$\delta_{\text{tot}} = \sqrt{\delta^2_{\text{sph}} + \delta^2_{\text{chr}} + \delta^2_{\text{spont}} + \delta^2_{\text{dip}} + \delta^2_{\text{diffr}} + \delta^2_{\text{source}}}. \tag{80}$$

The individual FWHM spot sizes are given by eqs. (45), (54), (69), (76), (78), and (79), respectively.

4 Examples

Before discussing specific examples, it is perhaps useful to consider the limitations imposed by keeping the lens in the first order, paraxial regime. As discussed in section 2.1, we require (a) $r^2 \ll w_o^2$, (b) $p_o = \mathcal{O}(1)$, (c) $U(r,z) \ll E_o$, and (d) $r' \ll 1$. Given the first two of these requirements, (c) reduces to $\hbar\Delta \lesssim E_o$. This is not much of a limitation on Δ, since $E_o/\hbar$ is usually of order $10^{13} - 10^{14}$ rad/s. By examining the slope of the trajectory at the focus, where it reaches its largest value, it can be shown that requirement (d) is satisfied as long as (a) is true. Clearly the most limiting restriction is requirement (a). This is especially true when small spot sizes are desired, since, as will be seen below, the ultimate spot size generally decreases as w_o decreases. Nanometer-size spot diameters will require very small values for w_o, which means the initial atom beam size r_o will need to be even smaller. We now discuss some numerical examples in order to provide a general understanding of the operating ranges of the donut mode laser-atomic lens. In all examples we consider the focusing of sodium atoms, using a laser tuned near the 3S–3P (D_2) transition. The wavelength of the transisition $\lambda = 0.59$ μm, the natural linewidth $\gamma = 6.28 \times 10^7$ rad/s, and the saturation intensity $I_s = 10\text{mW/cm}^2$, The mass m is 3.84×10^{-23} g. We calculate six cases, and also examine the minimum focal length condition. The six cases, originally selected by Gallatin and Gould,[6] (GG) are chosen with laser powers of 0.1 and 1.0 W for each of three atomic velocities, 1×10^4, 5×10^4, and 1×10^5cm/s. The laser beam waist w_o is kept at 1.0 μm, making the Rayleigh length $L = 5.33$ μm, and the detuning is chosen in each case such that $p_o = 2$.

4.1 First order properties

Using eq. (11) for q, and eqs. (18) and (19) for the principal plane locations and focal lengths, it is a simple matter to calculate the first order lens properties. Table 1 shows the results for the six cases discussed by GG, and Figs. 5(a) and (b) shows ray traces for each case. In cases A and D, we see that $q > 2$, corresponding to a lens with multiple crossovers. The trajectories shown in Fig. 5 illustrate this. The first principal planes are well removed from the center of the lens, so the lens is quite thick. Case C, on the other hand, is very close to a thin lens, since the focal length is long and the principal plane is near the lens center. Case E has the shortest focal length of the six cases, and f is close to the minimum value of 5.33 μm. Interestingly, this is true even though q is not very close to 2. Apparently, there is a relatively wide range of excitations for which the focal length is close to the minimum, but the principal plane is in different locations, as can be see in Fig. 3. This has design implications in that the minimum focal spot diameter, attained at the shortest focal length for a diffraction limited lens, can be realized over a broad range of excitations.

The last column in Table 1 contains the focal spot locations obtained by GG for a Gaussian atomic beam with a waist of radius 0.07 μm located at $z = -3L$. Excellent agreement is seen in all but the thickest lens cases A and D, where some deviation is apparent.

The minimum focal length trajectory, the "telescopic" case, is shown in Fig. 5(c). This occurs when $q = 2$, which results in $f = -z_p = L$ (5.33 μm for $w_o = 1.0$ μm). Given an initial atomic velocity, and a fixed p_o of order one (say $p_o = 2$) the laser power and detuning necessary to achieve the minimum focal length (MFL) condition

are uniquely determined. Using the expression for q (eq. 11), we can derive

$$\Delta^{\mathrm{MFL}} = \frac{3E_o}{\hbar}\frac{\lambda^2}{\pi^2 w_o^2}, \tag{81}$$

and

$$P_o^{\mathrm{MFL}} = \frac{18}{\pi^3}\frac{E_o^2}{\hbar^2\gamma^2}\frac{\lambda^4}{w_o^2}I_s, \tag{82}$$

where in the last expression we have neglected γ in the denominator of eq. (7). Table 2 shows the laser powers and detunings required for a MFL lens given the three initial velocities of the examples above. We note that for moderately low atomic velocities, the power required is quite small, but increases dramatically as the velocity is raised. This is because P_o^{MFL} depends on E_o^2, resulting in a v_o^4 dependence.

The strong v_o-dependence seen here should not be misinterpreted as causing a large chromatic aberration. It arises because the detuning is increased together with the velocity, requiring more laser power to keep p_o constant. In a real situation, Δ would be held fixed, in which case the chromatic aberration would be as discussed in Section 3.2.2.

4.2 Focal spot sizes

In this section we calculate the FWHM spot diameter contributions arising from each of the sources discussed in Section 3, using eqs. (45) (54), (69), (76), (78), and (79). Results are obtained for the six cases discussed above, and also for the minimum focal length condition. An initial beam radius r_o of 0.1 μm is assumed. For the source size aberration, we assume a source of radius 0.1 μm at a distance of 1 cm, which gives a collimation half-angle of 10^{-5}. For the chromatic aberration, we assume $\Delta E_{1/2}/E_o = 2 \times 10^{-3}$, in accord with Refs. [6] and [5]. Table 3 shows the results for each spot size contribution in nm in each of the six cases, as well as the quadrature

sum δ_{tot}. Several interesting features are apparent in the table. Generally, the largest contributions are diffraction, dipole fluctuations, and spherical aberration. At low initial velocity, diffraction is by far the dominant effect, while at high velocities, the dipole fluctuations become larger. Spherical aberration is larger at the higher velocities as well, becoming comparable to diffraction in cases C and F. Case E, in which the focal length is shortest, has the smallest net spot size, as expected. The chromatic aberration is very small in each case; however, this is somewhat arbitrary, since the spot size is proportional to $\Delta E_{1/2}/E_o$. The significance of this is that the restrictions on the fractional energy spread in the atom beam are not as severe as indicated in earlier work[5, 6]. A part in 10^2 could in principle be tolerated, as this brings the spot size contribution to the same order of magnitude as the other contributions.

To provide a comparison of the diffraction spot size with the results of Gallatin and Gould, we also consider the propagation of the Gaussian atomic beam with waist of radius 0.07 μm located at $z = -3L$. Our results for the $1/e^2$ waist diameters $2\sigma_o$ are given in Table 4, along with those of GG. Interestingly, the spot sizes are in excellent agreement for cases B, C, E, and F. Cases A and D do not show such good agreement. This could perhaps be explained by noting that the principal plane is located very far out of the lens in these two cases. Thus the waist position $z = -3L = -15.99$ μm cannot really be considered to be in a field free region in these cases, as was assumed by GG.

Spot sizes for the minimum focal length lens are shown in Table 5 for three initial atomic velocities. The laser power and detuning are those given in Table 2. At 1×10^4 cm/s, the lens is essentially diffraction limited. At the higher velocities, the

dipole fluctuation aberration grows as the contribution due to diffraction decreases, so that at a velocity of 1×10^5 cm/s, the contributions are about equal. The spherical aberration, chromatic aberration, and source size contributions are the same for each velocity because they depend only on parameters held fixed in the minimum focal length lens.

5 Lens optimization

One of the most useful applications of the explicit expressions for the various spot sizes obtained in this paper is lens optimization. By examining how each of the aberrations, diffraction, and the source size contribution depend on the laser and atomic beam parameters, it is possible to determine what combinations of parameters give the smallest spot size.

Presuming that a particular atom is chosen, so that the mass m, the wavelength λ, the resonant angular frequency ω_o, and the linewidth γ are fixed, there are seven "free" parameters to be optimized. The laser beam has three parameters available for optimization, i.e., the power P_o, the detuning Δ, and the waist size w_o. Instead of working directly with P_o and Δ, however, it is more convenient to work with the lens excitation parameter q and the spatially independent saturation parameter p_o. Though these parameters may seem interdependent, examination of the definitions shows that, given the freedom to choose any P_o and Δ, any values for q and p_o can be obtained.

The atom beam has four parameters which can in principle be selected for minimum spot size: the source size d_o, the beam radius at the lens r_o, the mean velocity v_o, and the energy spread $\Delta E_{1/2}$. Of the seven parameters available for optimization, three can be identified as not having specific values that minimize any of the spot size contributions. The parameter p_o has no effect on chromatic aberration, diffraction, or the source size effect, and its effect on the spherical, spontaneous and dipole aberrations is to reduce them monotonically as it decreases. The source size d_o only affects the source size contribution, which is directly proportional to it. The energy width $\Delta E_{1/2}$ is similar in that it has only a linear effect on the chromatic aberration.

To obtain the smallest possible spot size, the only option is to make these three parameters as small as practically possible, or small enough so that the contribution to the total spot size is negligible.

The remaining four parameters, q, w_o, r_o, and v_o affect the spot size contributions in different ways, causing some to increase, others to decrease, and having no effect on others. Thus it is reasonable to ask what values of these parameters give the smallest spot size.

First, let us examine the behavior of the net spot size as a function of the lens excitation q. All the aberrations, with the exception of chromatic, can be made arbitrarily small with sufficiently large q. The chromatic aberration decreases initially, but becomes constant for large enough q. The diffraction and source size contributions to the spot size, however, are smallest at the minimum focal length condition $q = 2$. Since diffraction and the source size are major contributions to δ_{tot} at the smallest spot sizes, it seems reasonable to choose $q = 2$ as an optimum value. Additionally, this gives the lens symmetry properties, i.e., the focal spot is at the center of the lens, which could be important for practical reasons.

Let us now let $q = 2$ and ask how the total spot size at the minimum focal length can be minimized with respect to w_o, r_o and v_o. The source size contribution is not affected by any of these three parameters, so we can ignore it for the present discussion. With $q = 2$, the remaining FWHM spot diameters can be written as

$$\delta_{\text{sph}} \approx \frac{9\pi}{1024}(p_o + 8)\frac{r_o^3}{w_o^2} \tag{83}$$

$$\delta_{\text{chr}} = \frac{3\pi}{16}\frac{\Delta E_{1/2}}{E_o} r_o \tag{84}$$

$$\delta_{\text{spont}} = \frac{\pi^{5/2}}{2}\sqrt{\frac{\ln 2}{6}}\left(\frac{\gamma p_o}{\lambda^5}\right)^{1/2}\frac{h}{m}\frac{w_o^2 r_o}{v_o^{3/2}} \tag{85}$$

$$\delta_{\text{dip}} = \frac{3\sqrt{91\ln 2}}{256} p_o \left(\frac{\lambda}{\gamma}\right)^{1/2} \frac{r_o^3}{w_o^3} v_o^{1/2} \tag{86}$$

$$\delta_{\text{diffr}} = 0.61\pi \frac{h}{m\lambda} \frac{w_o^2}{r_o v_o}, \tag{87}$$

where the spherical aberration spot size is approximated by only the first term in eq. (45). This is a good approximation because L is generally larger than w_o. With eqs. (83)-(87), we can write the square of the total spot size as

$$\delta_{\text{tot}}^2 = A\frac{r_o^6}{w_o^4} + Br_o^2 + C\frac{w_o^4 r_o^2}{v_o^3} + D\frac{r_o^6 v}{w_o^6} + E\frac{w_o^4}{r_o^2 v_o^2} \tag{88}$$

with

$$A = \left[\frac{9\pi}{1024}(p_o + 8)\right]^2 \tag{89}$$

$$B = \left[\frac{3\pi}{16}\frac{\Delta E_{1/2}}{E_o}\right]^2 \tag{90}$$

$$C = \frac{\pi^5 \ln 2}{24} \frac{\gamma p_o}{\lambda^5} \frac{h^2}{m^2} \tag{91}$$

$$D = \frac{819 \ln 2}{65536} \frac{\lambda}{\gamma} p_o^2 \tag{92}$$

$$E = 0.372\pi^2 \frac{h^2}{m^2\lambda^2}. \tag{93}$$

Optimization of the lens for minimum spot size now consists of minimizing eq.(88) with respect to the three free parameters w_o, r_o and v_o. This is best done numerically, especially since in any real situation, there will be constraints imposed on these parameters. For three simple examples, we consider a base case with $\delta_{\text{source}} = 0.11$ nm, $p_o = 2$, $\Delta E_{1/2}/E_o = 2 \times 10^{-3}$, $w_o = 1.0$ μm, $r_o = 0.1$ μm, and $v_o = 5 \times 10^4$ cm/s (i.e., the second case in Table 5). We let each of the three parameters vary in turn, while keeping the other parameters fixed. When w_o is free, a minimum spot of 1.11 nm is obtained at $w_o = 0.867$ μm. Allowing r_o to vary gives a minimum of 1.21 nm

at $r_o = 0.107$ μm. Varying v_o gives a minimum spot diameter of 0.835 nm with $v_o = 1.25 \times 10^5$ cm/s. These values show that the arbitrarily chosen examples in the previous section are fairly close to optimal.

6 Conclusion

We have shown that a donut mode laser-atomic lens can act as a focusing optical element for an atomic beam with very high resolution. By using particle optics techniques, we have derived simple expressions for the first order properties of the lens, and also all the major aberrations contributing to the spot size of a focused atom beam. Diffraction and source size contributions to the spot size are determined as well, and various examples are discussed. Using the expressions derived in this paper, optimization of the lens is shown to be possible.

The main purpose of this paper has been to provide a detailed description of the donut mode laser-atomic lens so that any future experimental work on such a lens will have a solid basis to build on. If attained experimentally, the focal spot sizes of approximately 1 nm discussed in this paper will open a wealth of new possibilities for nanostructure research, microscopy, and precision measurements. Though achieving some of the laser and atom beam parameters required for these spot sizes may push the limits of present technology, it is likely that in the near future they will be realizable.

7 Acknowledgements

The authors wish to thank the members of the Electron Physics Group at NIST, in particular Mark D. Stiles for stimulating conversations and Joseph A. Stroscio for assistance in generating Figure 1.

References

[1] J.E. Bjorkholm, R.R. Freeman, A. Ashkin, and D.B. Pearson, Phys. Rev. Lett. **41**, 1361 (1978).

[2] J.E. Bjorkholm, R.R. Freeman, A. Ashkin, abd D.B. Pearson, Opt. Lett. **5**, 111 (1980).

[3] V.I. Balykin, V.S. Letokhov, Yu.B. Ovchinnokov, and A.I. Sidorov, J. Mod. Optics **35**, 17 (1988).

[4] J.P. Gordon and A. Ashkin, Phys. Rev. A **21** 1606 (1980).

[5] V.I. Balykin and V.S. Letokhov, Opt. Comm. **64**, 151 (1987).

[6] G.M. Gallatin and P.L. Gould, private communication and J. Opt. Soc. Am. B (to be published).

[7] W. Glaser, Z. Physik **117**, 285 (1941) (see also Ref. [9]).

[8] See, e.g., H. Goldstein, *Classical Mechanics* (Addison-Wesley, 1950).

[9] P. Grivet, *Electron Optics*, 2nd ed. (Pergamon Press, Oxford, 1972).

[10] P.W. Hawkes and E. Kasper, *Electron Optics*, Vol. 1 (Academic Press, London, 1989).

[11] See also, e.g., A.B. El-Kareh and J.C.J. El-Kareh, *Electron Beams, Lenses, and Optics*, Vol. 2 (Academic Press, New York, 1970); M. Szilagyi, *Electron and Ion Optics* (Plenum Press, New York, 1988).

[12] See, e.g., J. Mathews and R.L. Walker, *Mathematical Methods of Physics* (W.A. Benjamin, Menlo Park, 1964), p. 8.

[13] See, e.g., R.K. Pathria, *Statistical Mechanics* (Pergamon Press, Oxford, 1972), p. 456 ff.

[14] J. Dalibard and C. Cohen-Tannoudji, J. Opt. Soc. Am. B **2**, 1707 (1985).

[15] M. Scheinfein and M. Isaacson, J. Vac. Sci. Technol. B **4** 326 (1986); M. Scheinfein, PhD Thesis, Cornell Univ. (1985).

Table 1

Case	v_o(cm/s)	P_o (W)	q	f (μm)	z_p (μm)	z_f (μm)	z_f (μm) (Ref. [6])
A	1×10^4	0.1	3.66	7.04	−11.64	−4.60	−3.9
B	5×10^4	0.1	1.22	9.85	−1.57	8.28	8.4
C	1×10^5	0.1	1.06	30.1	−0.46	29.7	29.9
D	1×10^4	1.0	6.33	11.20	−21.1	−9.86	−7.1
E	5×10^4	1.0	1.60	5.77	−3.57	2.20	2.3
F	1×10^5	1.0	1.18	11.59	−1.30	10.29	10.4

Table 1. First order properties of a TEM_{01}^* laser-atomic lens for sodium with $w_o = 1.0$ μm, $L = 5.33$ μm, and $p_o = 2$. f is the focal length of the lens, z_p is the position of the principal plane, and z_f is the position of the focal point for an initally parallel atom beam.

Table 2

v_o (cm/s)	P_o^{MFL} (W)	Δ^{MFL} (rad/s)
1×10^4	0.006	1.92×10^{11}
5×10^4	3.68	4.81×10^{12}
1×10^5	58.8	1.92×10^{13}

Table 2. Laser power and detuning necessary to achieve minimum focal length (MFL) conditions for three atomic velocities. Results are for sodium atoms, with $w_o = 1.0\ \mu$m and $p_o = 2$.

Table 3

Case	λ_{dB}	δ_{sph}	δ_{chrom}	δ_{spont}	δ_{dip}	δ_{diffr}	δ_{source}	δ_{tot}
A	0.172	0.06	0.105	0.087	0.015	7.40	0.14	7.40
B	0.0345	1.11	0.157	0.070	2.32	2.07	0.20	3.32
C	0.0172	1.75	0.184	0.105	5.04	3.17	0.60	6.24
D	0.172	0.02	0.102	0.160	0.001	11.8	0.22	11.8
E	0.0345	0.50	0.129	0.024	0.93	1.21	0.12	1.62
F	0.0172	1.24	0.163	0.032	3.67	1.22	0.23	4.07

Table 3. FWHM spot diameters in nm arising from each of the contributions discussed in this paper for the six cases of Table 1. Spherical aberration, δ_{sph}; chromatic aberration, δ_{chr}; spontaneous emission aberration, δ_{spont}; dipole fluctuation aberration, δ_{dip}; diffraction, δ_{diffr}; source size, δ_{source}. The fractional energy spread in the atom beam $\Delta E_{1/2}/E_o = 2 \times 10^{-3}$. The source radius is 0.1 μm, located at $z_o = -1$ cm. δ_{tot} is the quadrature sum of all contributions.

Table 4

Case	$2\sigma_o$	$2\sigma_o$(Ref. [6])
A	11.0	7.0
B	3.09	3.0
C	4.72	4.7
D	17.3	6.3
E	1.81	1.7
F	1.82	1.8

Table 4. Comparison with Ref. [6] (GG) of $1/e^2$ spot diameters $2\sigma_o$ for a Gaussian atomic beam. Diameters are given in nm at the focus for the six cases of Table 1, ignoring all other spot size contributions. A waist radius of $\sigma_o = 0.07$ μm located at $z = -3L = -15.99$ μm is assumed.

Table 5

v_o(cm/s)	δ_{sph}	δ_{chrom}	δ_{spont}	δ_{dip}	δ_{diffr}	δ_{source}	δ_{tot}
1×10^4	0.27	0.118	0.172	0.18	5.61	0.11	5.63
5×10^4	0.27	0.118	0.016	0.40	1.12	0.11	1.23
1×10^5	0.27	0.118	0.005	0.57	0.56	0.11	0.86

Table 5. FWHM spot diameters in nanometers at the minimum focal length condition for sodium atoms at three atomic velocities. Laser power and detuning are given in Table 2; $w_o = 1.0$ μm, $p_o = 2$. Spherical aberration, δ_{sph}; chromatic aberration, δ_{chr}; spontaneous emission aberration, δ_{spont}; dipole fluctuation aberration, δ_{dip}; diffraction, δ_{diffr}; source size, δ_{source}. The fractional energy spread in the atom beam $\Delta E_{1/2}/E_o = 2 \times 10^{-3}$. The source radius is 0.1 μm, located at $z_o = -1$ cm. δ_{tot} is the quadrature sum of all contributions.

Figure Captions

Figure 1. Laser focusing of atoms in a TEM_{01}^{*} ("donut") mode laser beam. Cross sectional view of the focus of the laser beam, with laser intensity represented by a gray scale. The atom beam propagates coaxially with the laser beam, being focused by the gradient in the laser intensity.

Figure 2. Sample trajectory, described by eq. (16), of an atom initially travelling parallel to the z-axis at a radius of 0.1 μm. The locations of the focal point and the principal plane are shown, along with the definitions of the angle ϕ and the focal length f. For this trajectory, $q = 1.42$.

Figure 3. Focal length f and principal plane location z_p as a function of q. Note THE focal length has a minimum at $q = 2$, where $z_p = -f$.

Figure 4. Trajectory $R_1(Z)$ used in determining aberration coefficients for finite object and image distances. The ray crosses the z-axis at the object position z_o with slope α_o, and again at the image position z_i with slope α_i. For this particular ray, $\alpha_o = 0.025$, $q = 1.15$, and $L = 5.32$ μm.

Figure 5. Ray traces of atomic trajectories through a donut mode laser-atomic lens. (a) Cases A-C of Table 1, $P_o = 0.1$ W, $v_o = 1 \times 10^4$, 5×10^4, and 1×10^5 cm/s. (b) Cases D-F of Table 1, $P_o = 1.0$ W, $v_o = 1 \times 10^4$, 5×10^4, and 1×10^5 cm/s. (c) Minimum focal length condition, with $q = 2$.

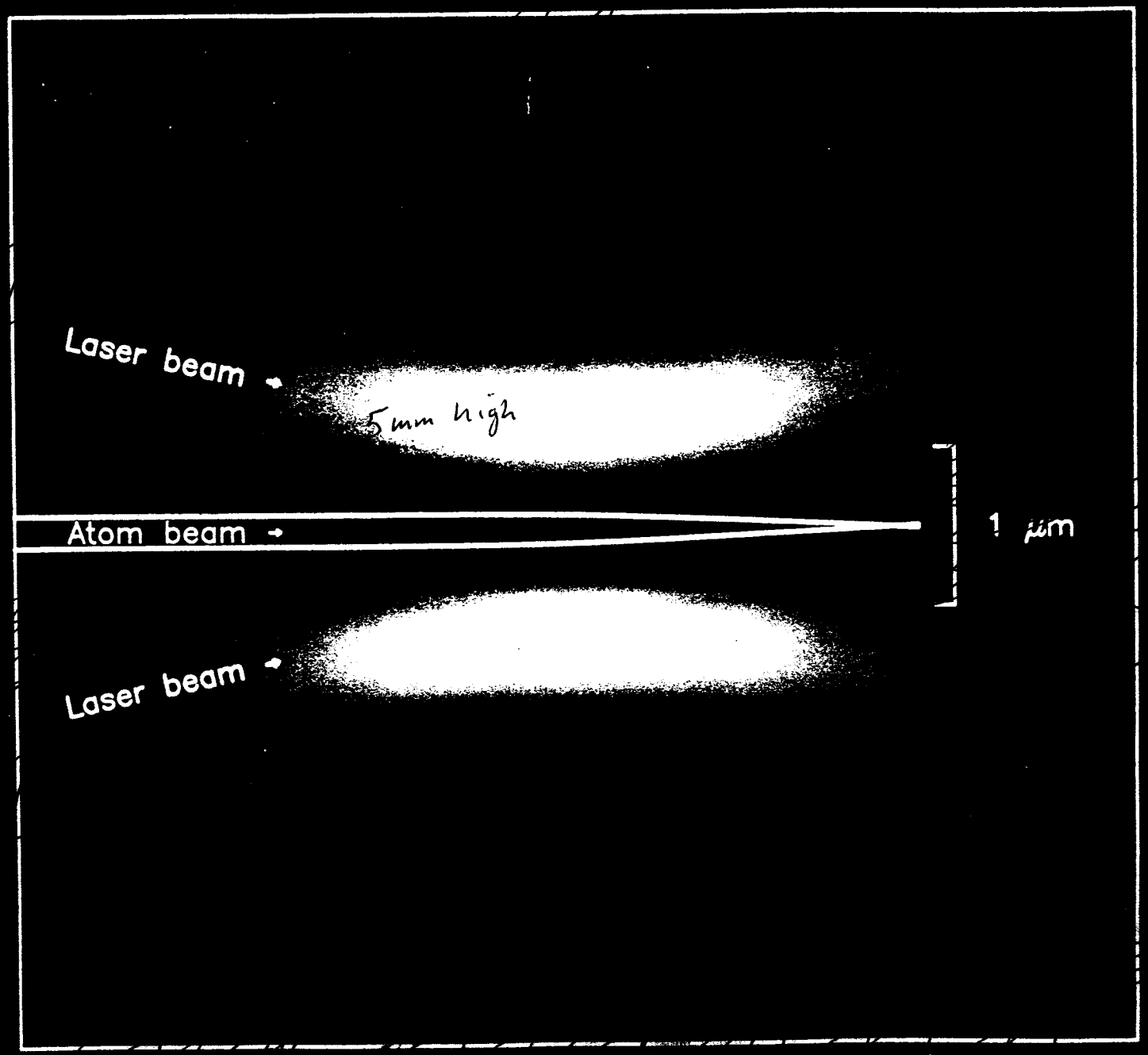

Cross sectional view of atom beam focusing using a "donut" mode laser beam

FIG 2

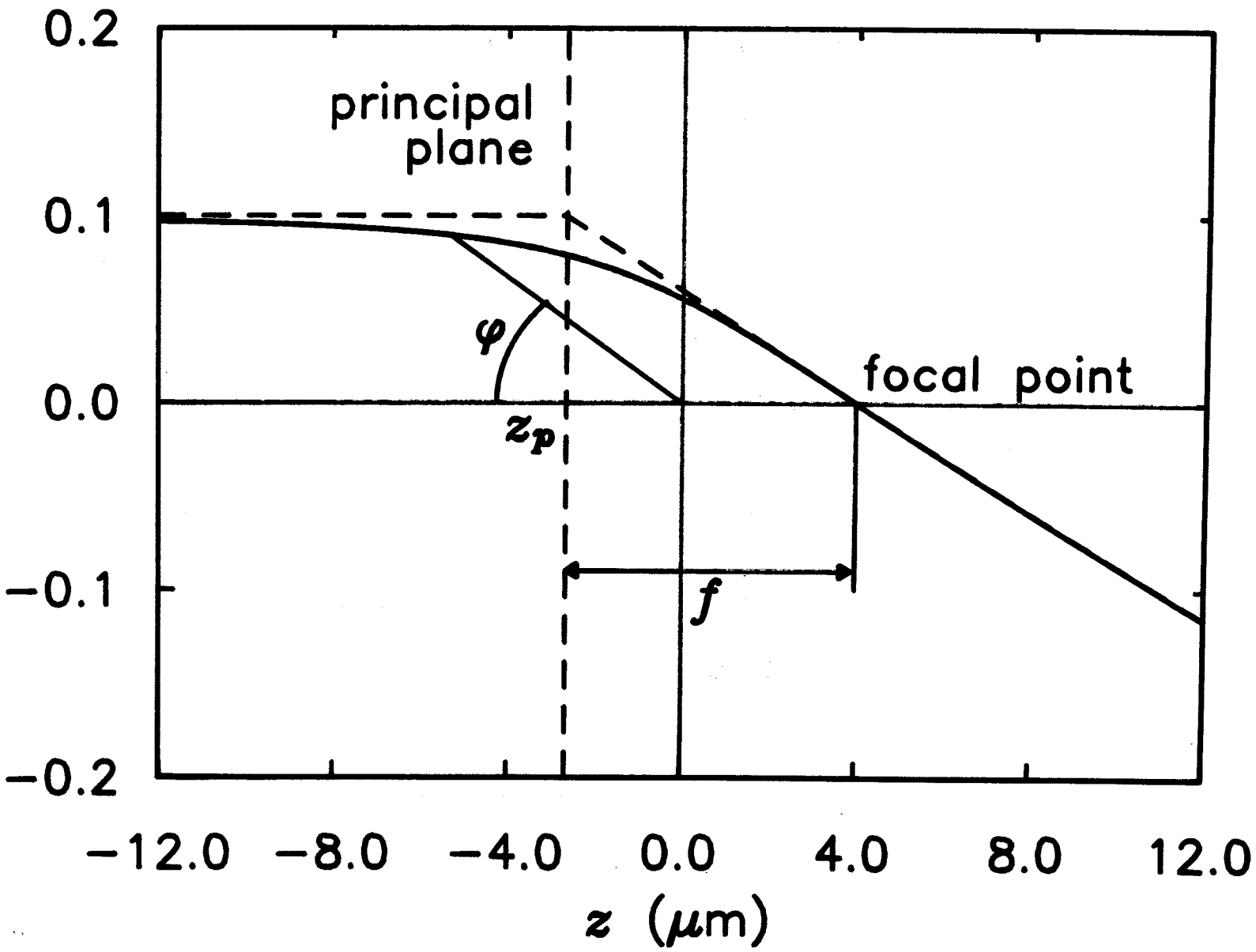
0.2
0.1
0.0
−0.1
−0.2
principal
plane
φ
z_p
focal point
f
−12.0
−8.0
−4.0
0.0
4.0
8.0
12.0
z (μm)

FIG 3

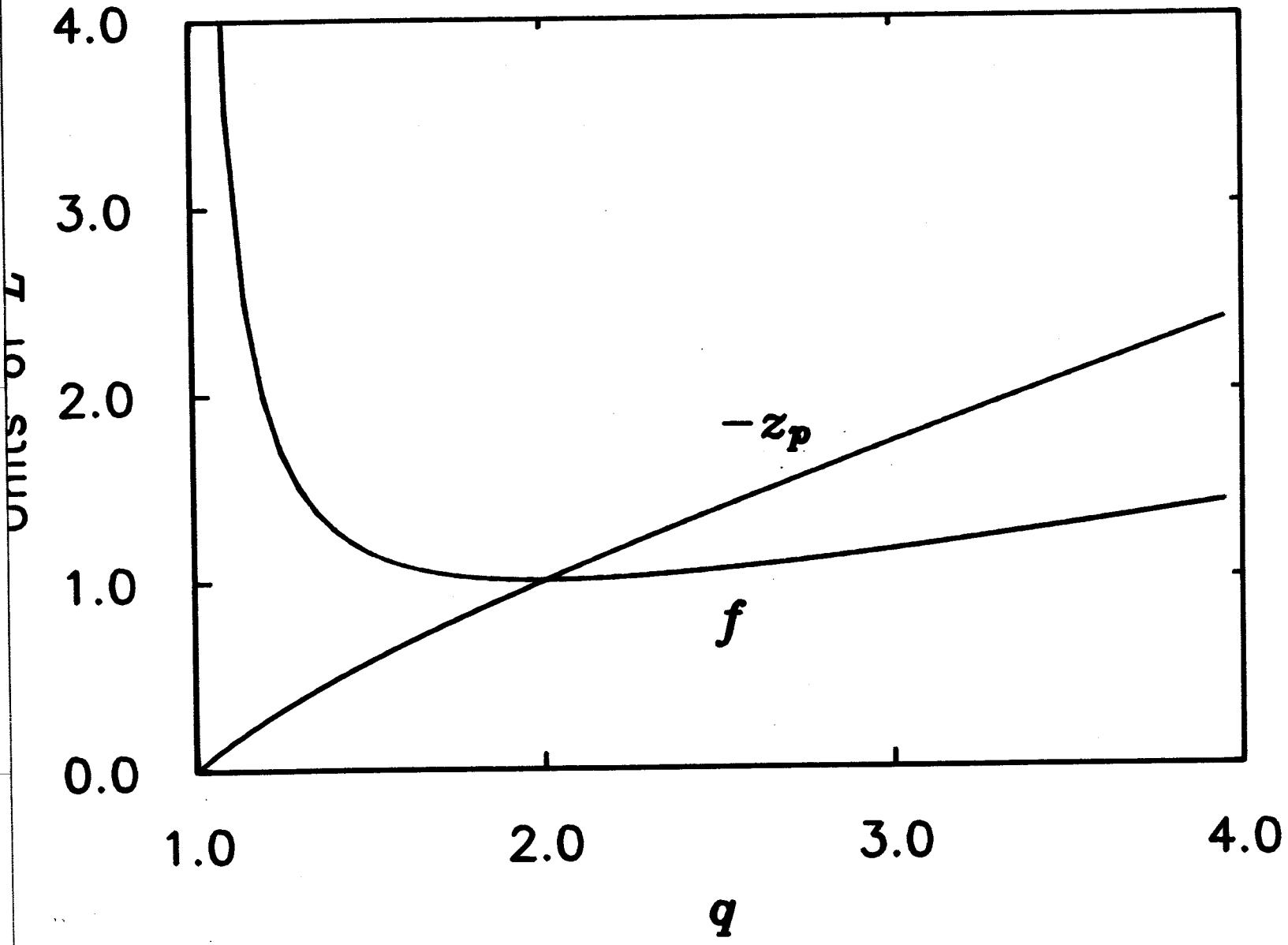

FIG 5

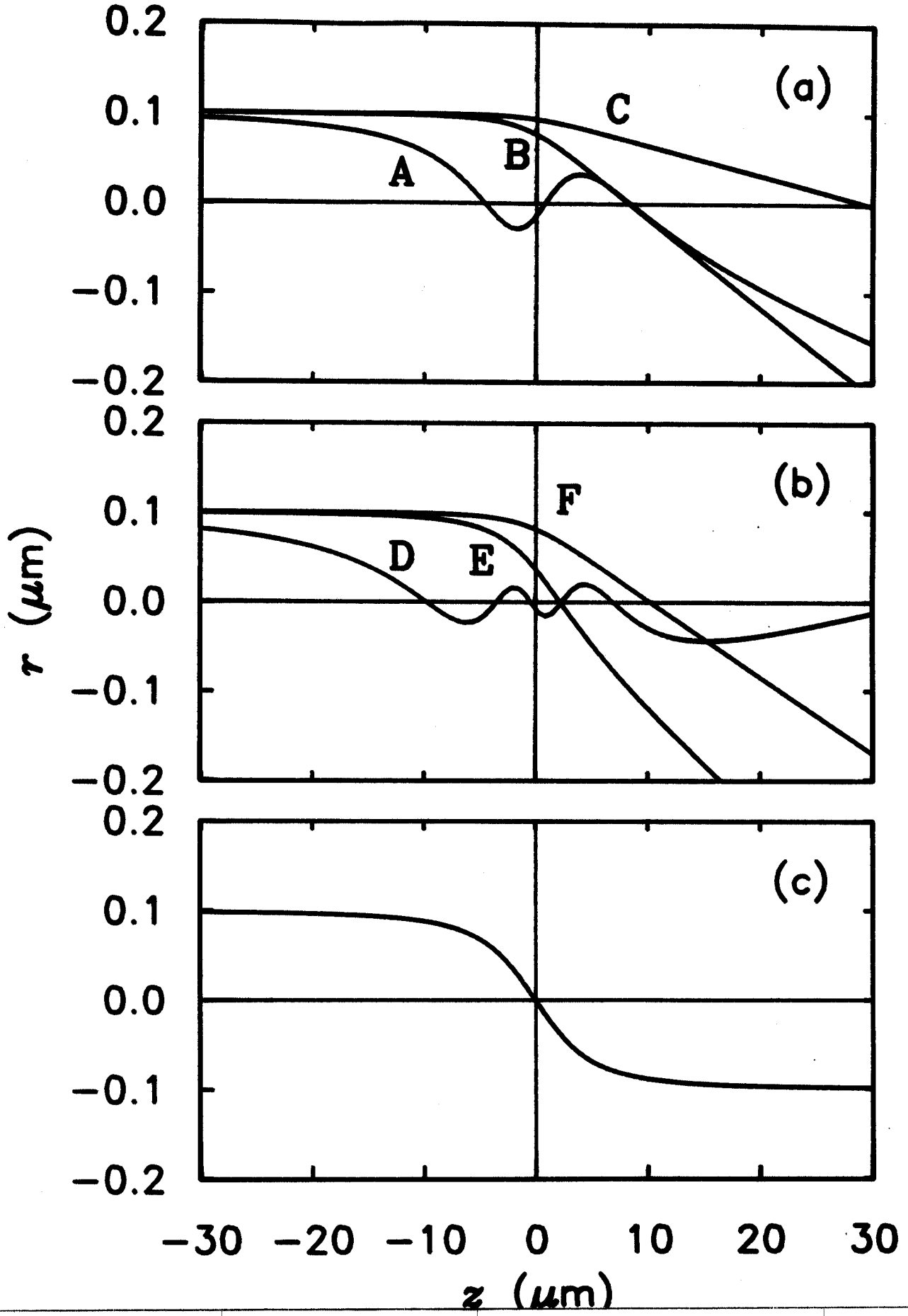

FIG 4

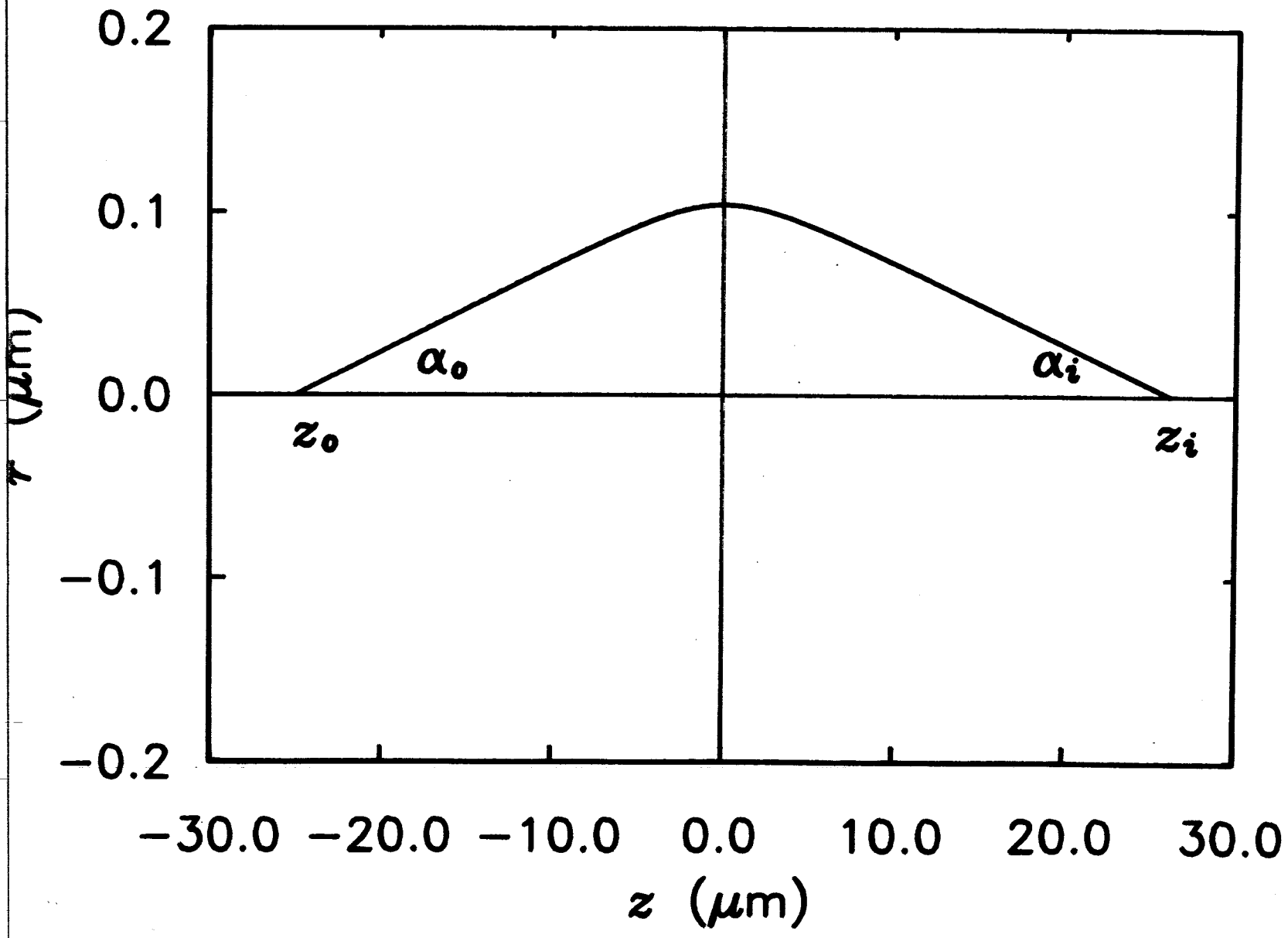
0.2
0.1
0.0
−0.1
−0.2
r (μm)
α_o
α_i
z_o
z_i
−30.0 −20.0 −10.0 0.0 10.0 20.0 30.0
z (μm)